

RESEARCH ARTICLE

Quantifiable correlation of ToF-SIMS and XPS data from polymer surfaces with controlled amino acid and peptide content

Michael Taylor^{1,2} | Fabio Simoes¹ | James Smith³ | Sivaneswary Genapathy¹ |
Anne Canning¹ | Marina Lledos¹ | Weng C. Chan¹  | Chris Denning⁴ |
David J. Scurr¹ | Rory T. Steven⁵ | Steve J. Spencer⁵ | Alexander G. Shard⁵  |
Morgan R. Alexander¹  | Mischa Zelzer¹ 

¹School of Pharmacy, University of Nottingham, Nottingham, UK

²Pacific Northwest National Laboratory, Richland, Washington, USA

³School of Medicine, University of East Anglia, Norwich, UK

⁴School of Medicine, University of Nottingham, Nottingham, UK

⁵National Physical Laboratory, Teddington, UK

Correspondence

Mischa Zelzer, School of Pharmacy, University of Nottingham, Nottingham NG7 2RD, UK.
Email: mischa.zelzer@nottingham.ac.uk

Funding information

EPSRC, Grant/Award Number: EP/F500491/1; Leverhulme Trust, Grant/Award Number: RPG-2016-199; Chemical and Biological Programme of the National Measurement System; EURAMET, Grant/Award Number: HLT04-REG4

Peptide-coated surfaces are widely employed in biomaterial design, but quantifiable correlation between surface composition and biological response is challenging due to, for example, instrumental limitations, a lack of suitable model surfaces or limitations in quantitatively correlating data from different surface analytical techniques. Here, we first establish a reference material that allows control over amino acid content. Reversible addition-fragmentation chain-transfer (RAFT) polymerisation is used to prepare a copolymer containing alkyne and furan units with well-defined chain length and composition. Huisgen Cu(I)-catalysed azide-alkyne cycloaddition reaction is used to attach the model azido-polyethyleneglycol-amide-modified pentafluoro-L-phenylalanine to the polymer. Different compositional ratios of the polymer provide a surface with varying amino acid content that is analysed by X-ray photoelectron spectroscopy (XPS) and time-of-flight secondary ion mass spectrometry (ToF-SIMS). Nitrogen-related signals are compared with fluorine signals from both techniques. Fluorine and nitrogen signals from both techniques are found to be related to the copolymer compositions, but the homopolymer data deviate from this trend. The approach is then translated to a heparin-binding peptide that supports cell adhesion. Human embryonic stem cells cultured on copolymer surfaces presenting different amounts of heparin-binding peptide show strong cell growth while maintaining pluripotency after 72 h of culture. The early cell adhesion at 24 h can be correlated to the logarithm of the normalised CH_4N^+ ion intensity from ToF-SIMS data, which is established as a suitable and generalisable marker ion for amino acids and peptides. This work contributes to the ability to use ToF-SIMS in a more quantitative manner for the analysis of amino acid and peptide surfaces.

KEYWORDS

cell-material interaction, heparin-binding peptide, human embryonic stem cells, peptide-polymer conjugates, surface analysis

This is an open access article under the terms of the Creative Commons Attribution License, which permits use, distribution and reproduction in any medium, provided the original work is properly cited.

© 2022 The Authors. *Surface and Interface Analysis* published by John Wiley & Sons Ltd.

1 | INTRODUCTION

Controlling cell response by modification of the physicochemical properties of the cellular environment is an attractive prospect in stem cell research as it provides the means to control stem cell fate (e.g., proliferation and differentiation). A cells' phenotypic response to its environment may initiate the expression of specific genes¹ or signalling pathways^{2,3} that influence cell response. For example, osteogenesis and adipogenesis may be promoted in human embryonic stem cell (hESC) cultures by phosphate and t-butyl containing surfaces.⁴ Understanding and controlling such cell–material interactions remains an active research area that requires improvement both in terms of biomaterial design and surface characterisation.

Bioactive materials harvested from native extracellular matrix such as laminin, fibrin and collagen are frequently used for cell-matrix studies as they are highly cell adhesive⁵; however, these types of naturally derived biomimetic materials (e.g., Matrigel⁶) suffer from non-negligible batch-to-batch variations in chemical composition and mechanical properties. Peptide sequences (e.g., RGD⁷, IKVAV⁸ and heparin-binding peptide [HBP]⁹) are frequently used in synthetic biomimetic materials to mimic a specific function in a controlled manner such as cell attachment to surfaces¹⁰ or self-renewal of cells.¹¹

HBPs possess the ability to bind heparin and other sulphated glycosaminoglycans within the extracellular matrix. They have been used on surfaces to bind and release cytokines and growth factors for wound healing,^{9,12} and they have been shown to support long-term hESC expansion.¹³ A systematic study that relates cell adhesion to quantitative surface analysis data that parametrise the amount of HBP on the surface has not yet been reported.

Quantitative surface analysis of peptide-coated surfaces is challenging, in part due to the compositional variability often inherent in biomaterial surfaces, and in parts due to the lack of well-defined model systems to provide a reference for analysis. Often, full surface coverage with the amino acid or peptide is not required or achieved^{14,15} as submonolayer coverage down to 2% can be sufficient to modulate cell response.¹⁶ These low amounts impose additional challenges on surface analysis methods as they require techniques with sufficiently high sensitivity and low detection limits. It is not uncommon in literature that successful surface modification is inferred mainly based on an observed effect on cell response to the material rather than a direct measurement.

A combination of surface analytical techniques is typically employed for the analysis of peptides on surfaces to complement the strengths and weaknesses of individual techniques. The quantitative nature and low surface penetration of X-ray photoelectron spectroscopy (XPS) and—in some instances—high sensitivity of time-of-flight secondary ion mass spectrometry (ToF-SIMS) make these two techniques a frequent choice for combined biomaterial surface analysis.^{15,17} Other techniques such as infrared¹⁸ and surface-enhanced Raman spectroscopy¹⁹ have also been explored, either alone or in combination with XPS or ToF-SIMS.

XPS is able to provide quantitative information on the relative amount of amino acids or, in some cases, peptides present on the

surface. The elements or chemical functionalities of interest must, however, be clearly resolved from the underlying material surface, not overlap with each other and be present in sufficient amounts to be detected (typical XPS detection limits are 1 to 0.1 at%, but can be better than 0.01 at% for elements with high photoionisation cross sections in a light-element matrix, e.g., fluorine in organic materials²⁰). Using powder samples of the amino acids Gly, Asp, Glu, His and Arg as references and the peptide sequences RGD, RGDS and RGDSC as model samples, Stevens et al showed that both qualitative and quantitative measurement of the amount and composition of peptide sequences is possible by XPS if the amino acids are sufficiently distinct from each other.²¹ Although this represents a significant advance in the data that can be extracted from XPS spectra of peptide surfaces, the approach is not universal for all amino acids. It requires correction for organic contaminants present on the surface and relies on sufficient signal strength from the amino acids and the ability to resolve and distinguish signal contributions from the substrate and the peptide that will be more difficult to achieve on small amounts of surface bound peptides than on powder samples.

ToF-SIMS has proven to be well suited to detect low amounts of amino acids or peptides on surfaces. Low surface amounts (submonolayer coverage) of single amino acids (e.g., Phe, Gly and Leu²²) and peptides such as RGD,^{23,24} RGDS²⁵ and phosphorylated RGDS²⁵ were detectable by ToF-SIMS and with the recent development of MS–MS capabilities for SIMS, proteins can also be identified.²⁶ Increasingly sophisticated tools such as machine learning algorithms²⁷ emerge to aid qualitative SIMS data interpretation and identification of amino acids and peptides. Due to the matrix effect, that is, the dependence of secondary ion intensities on the presence of other materials in the sample ion intensities derived from ToF-SIMS are generally not considered quantitative.²⁸ In some circumstances, it is possible to use ToF-SIMS data quantitatively with the help of a correction parameter that can be determined from samples for which the matrix effect is well understood to and accounts for the magnitude and sign of the matrix effect on a specific ion.²⁹

Attempts were made in the past to connect XPS data with ToF-SIMS data to enable more reliable quantification via ToF-SIMS, for example, to determine the relationship between thiol solution and surface layer composition in the formation of mixed self-assembled monolayers³⁰ or to interrogate the internal chemical distribution of submicron polymer-based particles.³¹ In a study that compares selected ion intensity ratios from ToF-SIMS with the O/C ratio or the %COOH obtained from oxidise polyethylene, no conclusive correlations between XPS and ToF-SIMS data were found.³² In contrast, calibration of principal components analysis (PCA) results from ToF-SIMS with the C/O ratio obtained by XPS from a plasma-treated polypropylene samples via partial least square regression showed some promising correlations.²⁸ Beer et al investigated the performance of XPS, ToF-SIMS and enzyme-linked immunosorbent assay (ELISA) for the quantification of amino acid and peptide ligands on a polymer hydrogel film and found that ToF-SIMS demonstrates higher sensitivity than XPS, allowing the use of ToF-SIMS to detect peptides at biologically relevant, low quantities that are not accessible by XPS.³³ The polymer

system used was an end-chain functionalised three-arm polyether that was formed into a hydrogel film, in which the amount of peptide ligand was modulated by varying the relative solution composition of polymer versus ligand.

In this study, we firstly address the challenge of developing a suitable amino acid-containing reference material to study XPS and ToF-SIMS data correlation. As many polymer-based biomaterials employ side-chain functionalisation in copolymers, we decided to develop a random copolymer-based system where ligand functionalisation is not solution controlled but modulated through the copolymer composition. Using controlled reversible addition-fragmentation chain-transfer (RAFT) copolymerisation and copper-catalysed azide-alkyne cycloaddition (CuAAC) click chemistry, we prepared a model surface that contains the amino acid Fmoc-pentafluoro-L-phenylalanine (pf-F). This amino acid contains fluorine atoms that are readily identifiable in both XPS and ToF-SIMS spectra and serve as internal reference of the model amino acid surface. Secondly, we used this model surface to investigate if a correlation can be established between the XPS and ToF-SIMS data from this model sample. Finally, the approach was translated to a biologically relevant system, an HBP-containing copolymer, to test the existence of quantifiable correlations between surface analysis data (XPS and ToF-SIMS) and cell expansion.

2 | EXPERIMENTAL

2.1 | Materials

3-(Trimethylsilyl)prop-2-yn-1-ol was purchased from Alfa Aesar (Haverhill, Massachusetts, US); methacryloyl chloride, 2-cyano-2-propyl dodecyl trithiocarbonate, tetrabutylammonium fluoride (TBAF), 2'-bipyridine, Tin(II) 2-ethylhexanate, CuBr, triethylamine (TEA), azobisisobutyronitrile (AIBN), 11-azido-3,6,9-trioxadecanamine, *N,N,N',N'*-tetramethyl-*O*-(1*H*-benzotriazol-1-yl)uronium hexafluorophosphate (HBTU), *N,N*-diisopropylethylamine (DIPEA) and furfuryl methacrylate were purchased from Sigma-Aldrich. Fmoc-pentafluoro-L-phenylalanine and azide-modified HBP were purchased from Bachem (Bubendorf, CH). Solvents (dichloromethane [DCM], methanol [MeOH], hexafluoroisopropanol [HFIP], dimethyl sulfoxide [DMSO] and dimethylformamide [DMF]) were purchased from Fisher Scientific (Pittsburgh, Pennsylvania, USA).

2.2 | Synthesis and polymer film preparation

2.2.1 | 3-(Trimethylsilyl) propargyl methacrylate (1)

Synthesis of the monomer was carried out according to the literature.³⁴ To a three-neck 250-ml round bottom flask, 3-(trimethylsilyl)prop-2-yn-1-ol (23.1 ml, 156 mmol), triethylamine (21.7 ml, 156 mmol) and diethyl ether (75 ml) were added. The mixture was then cooled down to -20°C before adding methacryloyl chloride (13.7 ml, 142 mmol) dropwise. The mixture

was left stirring overnight at room temperature. Once the reaction reached completion, the precipitate was removed by filtration, and residual solvent was evaporated in vacuo. Purification by flash chromatography (95:5 petroleum ether: ethyl acetate) resulted in a colourless oil (23.7 g, 85%).

^1H NMR (400 MHz, CDCl_3) δ /ppm: 6.12 (m, 1H, $\text{C}=\text{CH}_2$), 5.57 (m, 1H, $\text{C}=\text{CH}_2$), 4.71 (s, 2H, $\text{O}-\text{CH}_2$), 1.92 (s, 3H, CH_3), 0.13 (s, 9H, $\text{Si}-\text{CH}_3$).

^{13}C NMR (101 MHz, CDCl_3) δ /ppm: 166.67 (1C, $\text{O}-\text{C}=\text{O}$), 135.91 (1C, $\text{C}-\text{COO}$), 126.48 (1C, $\text{C}=\text{CH}_2$), 98.32 (1C, $\text{CH}_2-\text{C}\equiv\text{C}$), 92.05 (1C, $\text{C}\equiv\text{C}-\text{Si}$), 53.11 (1C, $\text{O}-\text{CH}_2$), 18.44 (1C, CH_3) and -0.14 (3C, $\text{Si}-\text{CH}_3$).

ToF MS ES^+ calculated for $\text{C}_{10}\text{H}_{16}\text{O}_2\text{Si}$: 196.03. Found: 197.0 $[\text{M} + \text{H}]^+$.

2.2.2 | 3-(Trimethylsilyl) propargyl methacrylate-ran-furfuryl methacrylate (50:50 monomer ratio) (P1)

A Schlenk tube was charged with **1** (500 mg, 2.55 mmol) and furfuryl methacrylate (424 mg, 2.55 mmol) and dissolved in toluene (5 ml). AIBN (1.3 mg, 0.008 mmol) and 2-cyano-2-propyl dodecyl trithiocarbonate (17.6 mg, 0.051 mmol) were then added to the tube before degassing the solution with argon for 30 min. The sealed Schlenk tube was then immersed into a preheated oil bath (70°C) to initiate polymerisation. The reaction was stopped at 7.5 h by exposing the solution to air and immersing the reaction vessel in ice. Purification was achieved by precipitation into cold methanol. Conversion (NMR): 82%, 360 mg recovered as a white powder.

^1H NMR (400 MHz, CDCl_3) δ /ppm: 7.41 (s, 1H), 6.37 (s, 1H), 6.33 (s, 1H), 4.94 (s, 2H), 4.56 (s, 2H), 1.81 (m, 4H), 0.83 (m, 6H), 0.17 (s, 9H).

Gel permeation chromatography (GPC) (CHCl_3 5% TEA): DP 41, M_n : 14.5 kDa, M_w : 19.9 kDa, M_w/M_n 1.37.

2.2.3 | Propargyl methacrylate-ran-furfuryl methacrylate (50:50 monomer ratio) (P2)

Copolymer **P1** (300 mg, 0.97 mmol of the alkyne unit) was added to a 25-ml flask and dissolved in tetrahydrofuran (4 ml). Acetic acid (0.08 ml, 1.46 mmol) was then added to the mixture. The solution was degassed with argon for 10 min and cooled to -20°C . One mole of solution TBAF in THF (1.5 ml, 1.46 mmol) was added dropwise via syringe and the mixture was stirred at -20°C for 30 min. The reaction was then allowed to warm up to room temperature and was stirred overnight. Once complete deprotection was achieved, the copolymer was purified by precipitation into cold methanol to obtain a white solid (190 mg), (**P2**).

^1H NMR (400 MHz, CDCl_3) δ /ppm: 7.41 (s, 1H), 6.38 (s, 1H), 6.33 (s, 1H), 4.92 (s, 2H), 4.56 (s, 2H), 2.46 (s, 1H), 1.80 (m, 4H), 0.83 (m, 6H).

GPC (CHCl₃ 5% TEA): DP 41, M_n: 12.7 kDa, M_w: 16.7 kDa, M_w/M_n = 1.31.

2.2.4 | (9H-Fluoren-9-yl)methyl (S)-(1-azido-13-oxo-15-(perfluorophenyl)-3,6,9-trioxo-12-azapentadecan-14-yl)carbamate (2)

Fmoc-pentafluoro-L-phenylalanine (500 mg, 1.05 mmol) and 11-azido-3,6,9-trioxoundecan-amine (200 µl, 0.87 mmol) were added to a 50-ml round bottom flask and dissolved in *N,N*-dimethylformamide (10 ml). HBTU (397 mg, 1.05 mmol) and DIPEA (282 mg, 2.18 mmol) were subsequently added to the flask, and this was left to stir at room temperature overnight. Once the reaction reached completion, the mixture was diluted and extracted with dichloromethane (3 × 25 ml). The organic phase was then washed with NaHCO₃, brine and 1-M HCl and dried over MgSO₄. The subsequent crude product was then concentrated in vacuo and purified by column chromatography (99.5:0.5 DCM:MeOH) to obtain a yellow waxy solid (335 mg, 57%).

¹H NMR (400 MHz, CDCl₃) δ/ppm: 7.76 (d, *J* = 7.5 Hz, 1H), 7.55 (dd, *J* = 7.2, 3.8 Hz, 1H), 7.40 (t, *J* = 7.4 Hz, 1H), 7.35–7.26 (m, 1H), 5.63 (d, *J* = 8.3 Hz, 1H), 4.45 (dd, *J* = 13.7, 7.8 Hz, 1H), 4.36 (dt, *J* = 25.8, 13.0 Hz, 1H), 4.27 (dd, *J* = 23.7, 13.2 Hz, 1H), 4.22–4.10 (m, 1H), 3.71–3.60 (m, 5H), 3.58–3.48 (m, 1H), 3.42 (dd, *J* = 39.0, 4.9 Hz, 2H), 3.35 (dd, *J* = 18.4, 13.5 Hz, 1H), 3.27 (dd, *J* = 14.1, 4.5 Hz, 1H), 3.08 (dd, *J* = 13.8, 8.2 Hz, 1H).

¹³C NMR (101 MHz, CDCl₃) δ/ppm: 299.08, 291.66, 273.20, 270.85, 257.33, 257.30, 256.64, 254.56, 249.54, 200.22, 200.17, 200.04, 199.79, 199.53, 198.92, 196.76, 188.14, 183.56, 180.23, 176.58, 169.06, 168.18, 167.44, 155.87, 129.56.

IR (Neat)/cm⁻¹: 3288, 3039, 2888, 2694, 2655, 2100, 1538, 1521, 1502, 1477, 1446, 1346, 1288, 1263, 1121, 1035, 973, 882, 726.

ToF MS ES + calculated for C₃₂H₃₂F₅N₅O₆: 677.23. Found: 678.20 [M + H]⁺ and 700.21 [M + Na]⁺.

2.2.5 | Amino acid-polymer conjugate (P3 pf-F)

Copolymer P2 (138 mg, 0.45 mmol of the alkyne unit) and azide 2 (335 mg, 0.49 mmol) were added to a 50-ml round bottom flask and dissolved in tetrahydrofuran (10 ml). The solution was degassed in nitrogen for 20 min, and CuBr (12.9 mg, 0.09 mmol) and 2',2'-bipyridine (28.11 mg, 0.18 mmol) were then added to the mixture under inert conditions. The reaction was stirred until the alkyne unit was completely converted to a triazole (24 h) and concentrated in vacuo. The mixture was then redissolved in a minimal volume of dichloromethane and precipitated into cold methanol dropwise. The copolymer was dried in high vacuum at room temperature overnight. A pale yellow solid (P3 pf-F) was recovered (175 mg).

GPC (CHCl₃ 5% TEA): DP 41, M_n: 20.2 kDa, M_w: 40.3 kDa, M_w/M_n = 1.99.

2.2.6 | Synthesis of HBP-polymer conjugate (10% peptide) click chemistry (P3 (HBP 10%))

Azide-terminated HBP (2) (40 mg, 0.02 mmol) was added to a 50-ml Schlenk flask and dissolved in dimethylsulfoxide (1.5 ml). Propargyl methacrylate-*ran*-furfuryl methacrylate (P2) (22 mg, 0.02 mmol) (10:90 monomer ratio) was added to the solution, which was degassed with nitrogen for 20 min while stirring. CuBr (0.5 mg, 0.003 mmol) and tin(II) 2-ethylhexanate (6.9 mg, 0.02 mmol) reducing agent were subsequently added. The solution was then stirred at room temperature for 3 days. Purification was carried out by precipitating the reaction crude dropwise onto cold diethyl ether. Residual copper was removed by redissolving the purified material in DMSO and passing the solution through a short column of neutral alumina. Twenty-five milligrammes were obtained as a pale yellow gum.

GPC was not taken due to poor solubility. The compound was characterised by NMR (Figure S18), and the films were analysed with XPS and ToF-SIMS.

IR (HFIP)/cm⁻¹: 3309, 3268, 2914, 2160, 1732, 1661, 1601, 1542, 1434, 1285, 1181, 1140, 1070, 957, 845, 678.

2.2.7 | Dip coating

Polymers were dissolved in chloroform or hexafluoroisopropanol (10 mg/ml) for the single amino acid and HBP, respectively. Glass cover slips were sonicated subsequently in water, acetone and methanol (15 min each), then dipped in solution using a HO-TH-01 dip coating unit (Holmarc Optomechatronics PVT. Ltd., Kochi, India). Retraction speed: 1 mm/s. Dip duration: 1 s. Dry duration: 60 s.

2.3 | Instrumentation

2.3.1 | Nuclear magnetic resonance

Spectra were acquired with a DPX400 UltraShield™ 400-MHz spectrometer (Bruker, Billerica, Massachusetts, USA). Spectra were analysed using MestReNova v14.2.1 software. Polymer conversion was calculated by monitoring peak integration ratios between a specific monomer peak and the correspondent polymer peak.

2.3.2 | Gel permeation chromatography

GPC was carried out with a GPC 50 (Polymer Laboratories Ltd., Church Stretton, UK) in a system equipped with two Polargel L 5-µm Mix D columns (Agilent, Santa Clara, California, US) and refractive index (RI) detector calibrated with Easivial polystyrene standards (162–371, 100 g/mol) from Polymer Laboratories Ltd., Church Stretton, UK, using chloroform/triethylamine 95:5 vol/vol as the mobile phase. For the DMF mobile phase, the system was calibrated with linear polymethylmethacrylate.

2.3.3 | Mass spectrometry

Mass spectrometry was carried out using a Micromass LCT KC453 spectrometer and Shimadzu (Kyoto, JP) API 2000 LC/MS/MS with Phenomex (Torrance, California, USA) Gemini NX 3- μ m-110A C18 column. Compounds were dissolved in methanol at 20 mg/ml. Acetonitrile/water 98:2 vol/vol was used as the mobile phase. Pre-equilibration was run for 1 min at 5% acetonitrile. Following this, the mobile phase was ramped to 98% acetonitrile over 2 min.

2.3.4 | Infrared spectroscopy

Infrared analysis was carried out using a Nicolet IR 200 FT-IR (Thermo Fisher Scientific, Waltham, Massachusetts, USA), using 32 scans at 8-cm⁻¹ resolution. The spectra were analysed with Omnic 8.0© 1992–2008.

2.3.5 | X-ray photoelectron spectroscopy

Surfaces were analysed using a Kratos (Manchester, UK) Axis Ultra XPS instrument featuring a monochromated Al K _{α} X-ray source producing photons of 1486-eV energy and operated at 75 W. Three wide scans (step size 1 eV, pass energy 160 eV and dwell time 200 ms) and three high-resolution scans (step size 100 meV, pass energy 20 eV and dwell time 500 ms) with two sweeps each were recorded from each sample using charge neutralisation. Each surface was measured in duplicates with three repeat measurements per sample for pf-F surfaces and at least two repeat measurements per sample for HBP surface. The data were processed with CasaXPS (v2.3.12) using a previously established transmission function³⁵ and average matrix relative sensitivity factors. Wide scan and high-resolution C1s spectra were energy referenced to the F1s signal (688 eV) or, in the absence of a F1s signal in the sample, the C1s signal (285 eV). Peak fitting was performed using five components: aromatic carbons (C=C; varied shift constraints, see Table S2); aliphatic carbons (C—C/C—H; set at 285 eV); amines and esters (C—N/ C—O—C, varied shift constraints, see Table S2); fluorinated carbons (C—F; no constraints) and carboxylic acids/esters and amides (C(=O)OX/ C(=O)N where X is either H or C; no constraints). All peaks were fitted using a GL (30) function. Peak fits carried out on the homopolymers (**P3 (pf-F 0%)** and **P3 (pf-F 100%)**) showed that the binding energy shift of aromatic carbons and amines/esters depended on the polymer composition. Although the energy separation between the C—C/C—H and C=C components is small such that these components would normally be fitted using a single peak, here we found that use of a single C—C/C—H/C=C peak reduces reproducibility of the fitting procedure. Fitting C—C/C—H and C=C in separate peaks increased reproducibility and allowed application of the same fitting parameters and constraints to all polymer surfaces. For the copolymers, the peak position for the C=C and C—N/C—O—C components was therefore fixed to binding shifts that were determined by weighting the binding shift contribution using the

binding energy shifts of the homopolymers and the theoretical composition of the copolymers. The resulting shifts are reported in Table S2, and the results of the fitting were tested by plotting the percentage of fluorinated carbons (C—F) against the percentage of fluorine detected on the wide scans (Figure S7).

2.3.6 | Time-of-flight secondary ion mass spectrometry

Nineteen millimetres dip-coated polymer cover slips were analysed on a ToF-SIMS IV time-of-flight instrument by IONTOF (Münster, Germany) using a Bi₃⁺ liquid metal ion gun in bunch mode at 25 keV (approximately 0.3-pA pulsed target current with a total primary ion dose of 9.2×10^{10} ions/cm²). A flux of low energy electrons (20 eV) was used for charge compensation. For each condition, three separate areas were measured on a single sample. Samples used for ToF-SIMS were different from those used for XPS but prepared in the same batch. Data processing was done with the commercial IONTOF software, SurfaceLab 6. Images were obtained by rastering the primary ion beam over 200 \times 200 μ m areas for pf-F samples (512 \times 512 pixels) or 1 \times 1 mm areas for HBP samples (256 \times 256 pixels). Secondary ion assignments were selected by referring to a reference database³⁶ of secondary ions related to the components of the material analysed.

2.4 | Embryonic stem cell attachment and expansion

Substrates in 24-well plate format were washed three times with 70% ethanol followed by three sterile PBS washes. Following air drying, substrates were exposed to mouse embryonic fibroblast (MEF) conditioned media containing 10% foetal bovine serum and 1% penicillin/streptomycin, for 1 h at 37°C with 5% CO₂ prior to cell seeding. The hESC line HUES7 was cultured on Matrigel (BD Biosciences, Franklin Lakes, New Jersey, US) substrates in MEF conditioned media, for no higher than passage 35, prior to seeding on samples. Passaging of cells was achieved by incubation with Accutase (Invitrogen, Waltham, Massachusetts, US) for 3 min at 37°C, with tapping of the flasks to dissociate cells. HUES7 cells were seeded at 100,000 cells per sample and incubated at 37°C with 5% CO₂ for 24 h to allow cell adhesion. Media was exchanged daily for a period of 72 h to allow cells to expand on substrates. To accurately determine adherent viable cell number at 24- and 72-h time points, samples were washed gently twice with PBS, then exposed to the CellTiter-Glo[®] Luminescent Cell Viability Assay (Promega, Madison, Wisconsin, US) following the manufacturer's instructions. Following 72 h of culture on substrates, adherent cells were fixed in 4% paraformaldehyde (Sigma-Aldrich, St. Louis, Missouri, US) and immunocytochemistry staining performed with OCT4 (SC-5279, Santa Cruz Biotechnology Inc., Dallas, Texas, US), NANOG (AF1997) and SOX2 (AF2018) (R&D Systems, Minneapolis, Minnesota, US)

antibodies to demonstrate maintenance of pluripotency. Three repeat measurements were taken.

2.5 | Statistical analysis

Trendlines for all data were fitted and the coefficients of correlation, Pearson's r values and analysis of variance (ANOVA) statistics were performed with OriginPro 2015 (OriginLab). One-way ANOVA for cell count results was performed in IBM SPSS Statistics v26 (IBM).

3 | RESULTS AND DISCUSSION

3.1 | Preparation of model polymer surfaces with defined amino acid content

3.1.1 | Polymer synthesis

To establish ToF-SIMS as a quantitative technique for peptide surface analysis, XPS data were used as a quantitative reference technique. Such a comparison and correlation of data from XPS and ToF-SIMS measurements requires samples that display a large degree of uniformity in their surface composition (i.e., amino acid or peptide density) both laterally and within the analysis depth probed by both

instruments. We therefore designed a copolymer system that could (i) be functionalised with both model ligands and biologically relevant ligands, (ii) display different and controlled degrees of functionalisation and (iii) allow formation of films thicker than the analysis depth of XPS. To establish the analytical procedures, we chose to work with a model amino acid ligand, an azido-PEG-amide-modified, Fmoc-protected pentafluoro-L-phenylalanine (pf-F), before translating the procedures to a more biologically relevant ligand, a HBP with the sequence GKKQRFHRNRKG (Figure S1).

Copolymer **P1** was synthesised from a trimethylsilyl-protected alkyne containing methacrylate (**1**) and a furan-modified methacrylate using RAFT polymerisation (Figure 1).³⁷ The second monomer has previously been shown to be biocompatible and acts as a filler to control copolymer composition, whereas the alkyne side group in the first monomer provides convenient anchor points for further modification with amino acids or peptides via CuAAC click chemistry after removal of the protecting group (**P2** and **P3**). The polymerisation kinetics were determined (Figure S2) and used to calculate the required reaction time for 80% conversion. Synthesis of the polymers was confirmed by NMR (Figure 2) and GPC (Figure S3). GPC analysis of copolymer **P1** identified isolation of a 19.9-kDa polymer with a low polydispersity (D) of 1.37, indicating that the RAFT polymerisation was successful. NMR indicated that the trimethylsilyl protecting group (CH_3 protons at 0.13 ppm) remained intact during the polymerisation. Upon removal of the trimethylsilyl protecting group from **P1**, the NMR

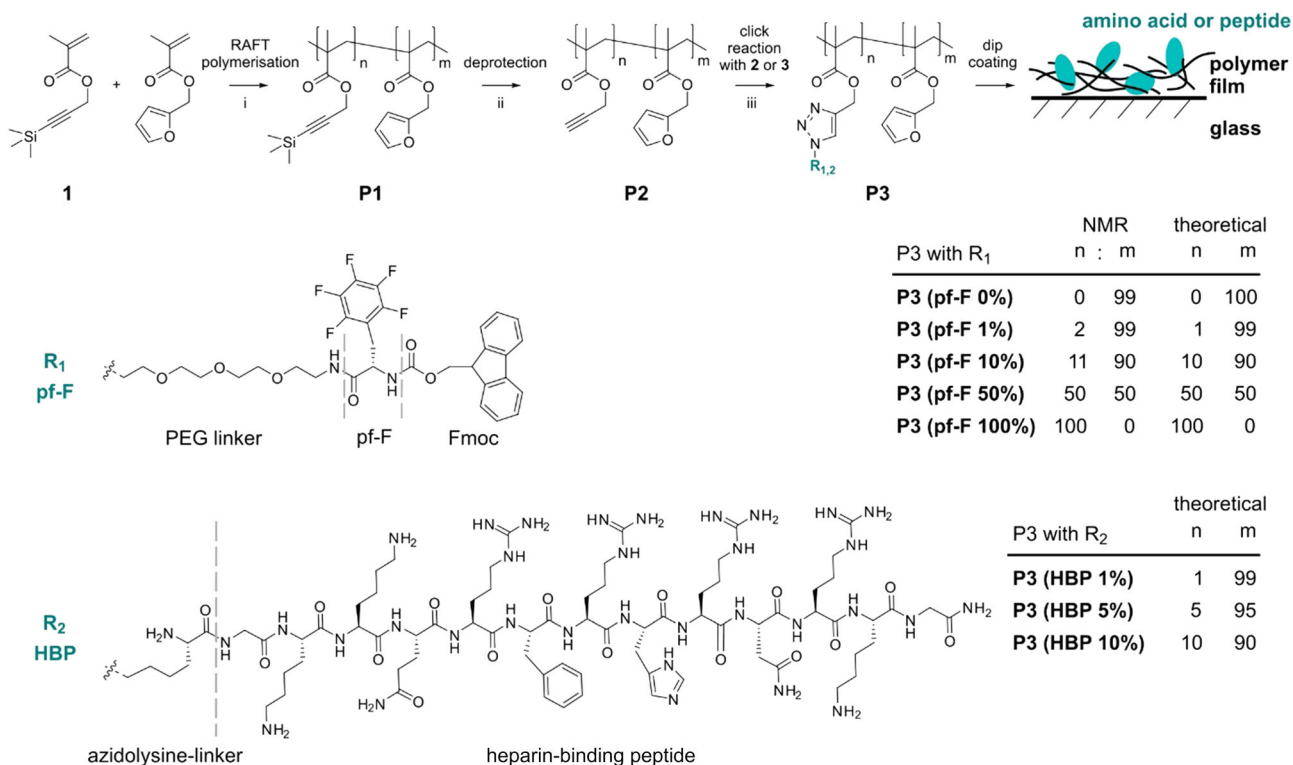


FIGURE 1 Synthetic route to prepare polymers with well-defined amino acid or peptide content and subsequent fabrication of amino acid or peptide-containing polymer films. Reaction conditions: (i) 2-cyano-2-propyl dodecyl trithiocarbonate, toluene, AIBN, Ar, 70°C; (ii) acetic acid, TBAF, THF, Ar, -20°C; (iii) CuBr, 2,2'-bipyridine, THF, Ar

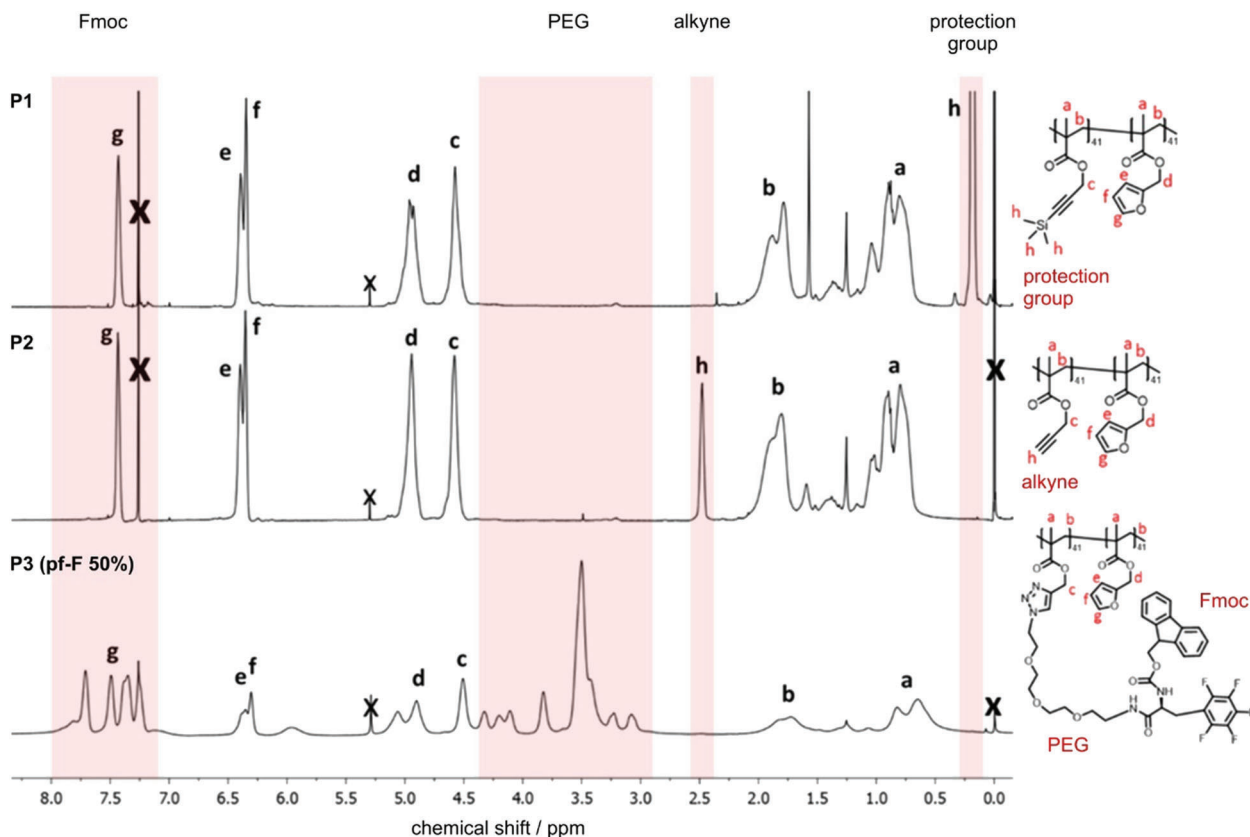


FIGURE 2 ^1H NMR spectra showing the stepwise side chain modification of the $n = m = 41$ polymer. Peak labels (a–g) represent protons in differing chemical environments from **P1** to **P3** (pf-F 50%), the corresponding structures of which are shown to the right of the spectra. **P1–P3** (pf-F 50%) TMS reference peak at 0 ppm is represented by x, as is CH_2Cl_2 at 5.32, and CHCl_3 is shown at 7.26 in **P1** and **P2**. The three spectra were recorded in CDCl_3

spectra showed complete disappearance of the methyl protons and the appearance of the terminal alkyne proton at 2.48 ppm in **P2**. The higher retention time of **P2** compared with **P1** measured with GPC indicates a decrease in the molecular weight of the polymer, showing that deprotection was successful.

To create model amino acid functionalised materials, Fmoc-pentafluoro-L-phenylalanine was functionalised with a C-terminal azide-PEG-amide group to provide compound (**2**). This enabled Cu(I)-mediated click reaction between pf-F and polymer **P2** to yield amino acid/copolymer conjugates with different degrees of functionalisation (variations of **P3** (pf-F) as shown in Figure 1). The Fmoc-protected analogue of pentafluoro-L-phenylalanine was chosen because fluorine is readily distinguishable in XPS and ToF-SIMS via its fluorine atoms and it is not a typical sample contaminant. The side-chain functionalisation was accommodated by an increase of the molecular weight of the polymer (Figure S3). The absence of the azide band at 2186 cm^{-1} in the IR spectra (Figure S4) suggests that no detectable unreacted pentafluoro-L-phenylalanine derivative remained in the material. The complete disappearance of the alkyne proton at 2.5 ppm in the NMR spectrum (Figure 2) further indicates that all alkyne groups have been functionalised with pf-F.

To obtain materials containing different, well-controlled amounts of amino acid, copolymers with varying relative numbers

of alkyne and furan units were prepared. By varying the molar ratios of 3-(trimethylsilyl)prop-2-yn-1-ol to furfuryl methacrylate ($n : m$) monomers in the reaction, copolymers with 0, 1%, 10%, 50% and 100% of the alkyne functionality for coupling of pf-F were obtained. The relative amount of pf-F side groups in the final polymers **P3** was determined by NMR, using the CH_2 signals of the ester group, which could be clearly distinguished from the other signals (Figure S5). Theoretical and measured compositions generally matched very well but showed small deviations (approximately 1%) for the copolymers containing low amounts of pf-F (Figure 1).

3.1.2 | Preparation of amino acid-containing polymer surfaces

The polymers were prepared as films on cleaned glass slides for surface analysis by XPS and ToF-SIMS. Surface profilometry showed that film thicknesses were uniform and ranged from approximately 0.5–0.8 μm . Although these measurements were taken under ambient conditions, the thickness of the films suggests that the polymer films are likely to persist for the full analysis depth of XPS and ToF-SIMS under vacuum conditions.

As surface analytical techniques and NMR provide different information and have different sensitivity and detection limits, we carried out XPS analysis on films of **P1**, **P2** and **P3 (pf-F 50%)** to investigate if any residual signals related to incomplete conversion could be detected (Figure S6 and Table S1). Deprotection of **P1** to **P2** was evident by the drastic decrease of the Si2p signal originating from the trimethylsilyl group, but traces of Si were still present on the **P2** and **P3** films. Although this suggests that either deprotection was not complete or that some signals from the underlying glass substrate may be present in the spectra, the total amount of Si in the final material is very low and can be assumed to have little effect on the surface analysis. The presence of pf-F in **P3 (pf-F 50%)** was indicated by the appearance of F1s and N1s signals, which are uniquely introduced in the sample by the model amino acid derivative.

As copper salt(s) may be introduced by the click reaction, and its presence on the films may affect biological responses, removal of copper is essential. No significant amounts of copper were detected by XPS on any samples, indicating that purification of the polymers was successful in removing copper ions.

3.2 | Comparison of ToF-SIMS and XPS data from surfaces with varying amino acid content

XPS and ToF-SIMS were used to obtain qualitative and quantitative information from the model amino acid films to answer two questions. Firstly, we investigated how well the expected (theoretical) material compositions matched the experimental XPS data. Secondly, we established if the material composition can be quantitatively measured by ToF-SIMS. For this second objective, we used fluorine as a unique marker, but we also compared nitrogen-containing signals from XPS and ToF-SIMS with fluorine signals to determine if nitrogen-based signals are sufficient to describe the change in amino acid composition. If this is the case, it would allow us to explore the use of nitrogen-based signals in peptide systems that do not contain unique markers.

3.2.1 | Theoretical versus experimental composition determined by XPS

XPS spectra of the polymer-amino acid conjugate films **P3 (pf-F 0–100%)** are shown in Figure 3. Carbon (C1s) and oxygen (O1s) signals originate from both the pf-F side group and the copolymer backbone and are present in all spectra. Increasing amounts of pf-F in the film were accompanied by increasing F1s and N1s peak intensities for a pf-F content up to 50%. For the 100% pf-F sample, both the F1s and N1s peak intensities decreased below that of the 50% pf-F sample (Table S1). The amounts of silicon detected were generally very low and comparable with the levels detected on the control sample (**P2**), suggesting that no significant contributions to the spectra can be expected from the glass substrate.

To further confirm the chemical composition of the films, peak fitting was carried out on the high-resolution C1s spectra (Figures S6 and 3). Due to the complex and varying composition of the spectra related to the diverse chemical environments present in the polymer-amino acid conjugates, a number of chemical environments (amines and ethers; carboxylic acids, esters, amides and carbamates) could not readily be distinguished from each other and were combined into single fitted peaks. In addition, the fitted components clearly showed the presence of C—F (from pentafluoro-L-phenylalanine) and C=C (from Fmoc, pentafluoro-L-phenylalanine and furan). As the binding energy shifts for similar chemical environments are different for the two monomer units, the peak positions were affected by the copolymer position, requiring imposition of some constraints that take the varying composition into account. The constraints used are provided in Table S2 and were derived based on the chemical shifts observed in the homopolymers, which were adjusted proportionally based on the theoretical composition of each copolymer. The resulting relative amount of each fitted component is provided in Table S3. The goodness of fit was tested by plotting the amount of C—F obtained from the component fitting against the relative amount of F1s detected in the wide scan spectra (Figure S7). The correlation fits a linear trendline ($R^2 = 0.984$) and has a statistically significant (ANOVA, $p = 0.057$) positive association (Pearson's r value = 0.996, Table S15) between the amount of F from the survey spectra and the amount of C—F from the fitted high-resolution spectra, suggesting that the fitting parameters are appropriate.

The types of components fitted match the expected chemical environments very well. A continuous increase in the amount of C—F and C=C bonds was observed when the pf-F content increased from 0 to 100%, except for the **P3 (pf-F 100%)** where the amount of C—F dropped compared with the **P3 (pf-F 50%)** sample (Table S3). However, when compared with the theoretical values, it is apparent that the relative amount of C—F is lower than expected, which matches the observation of an overall decrease in F1s peak intensity in the survey spectra.

To determine how the experimental XPS data matches expected theoretical compositions and understand the unexpected behaviour of the **P3 (pf-F 100%)** sample better, N/C, F/C and F/N atomic ratios were determined both from experimental XPS data and from the theoretical (co)polymer compositions (Table S4). The F/N ratio should be close to 1 for all pf-F containing samples. The average experimental values deviate slightly from the expected ones, but this can in general be attributed to measurement errors, in particular for samples where very low amounts of pf-F are present.

The N/C and F/C ratios can be used as a measure of how well the experimental data fits the expected polymer composition (Figure 4). Comparison of the experimental XPS data with the theoretical pf-F content (Figure 4A) suggest an increasing trend for the three copolymer samples (**P3 (pf-F 1%)**, **P3 (pf-F 10%)** and **P3 (pf-F 50%)**) but the homopolymers (**P3 (pf-F 0%)** and **P3 (pf-F 100%)**) deviate from linearity. A similar trend was observed when plotting experimental and theoretical values for the N/C and F/C ratios and the relative amounts of C—F and C=C bonds (Figure S8).

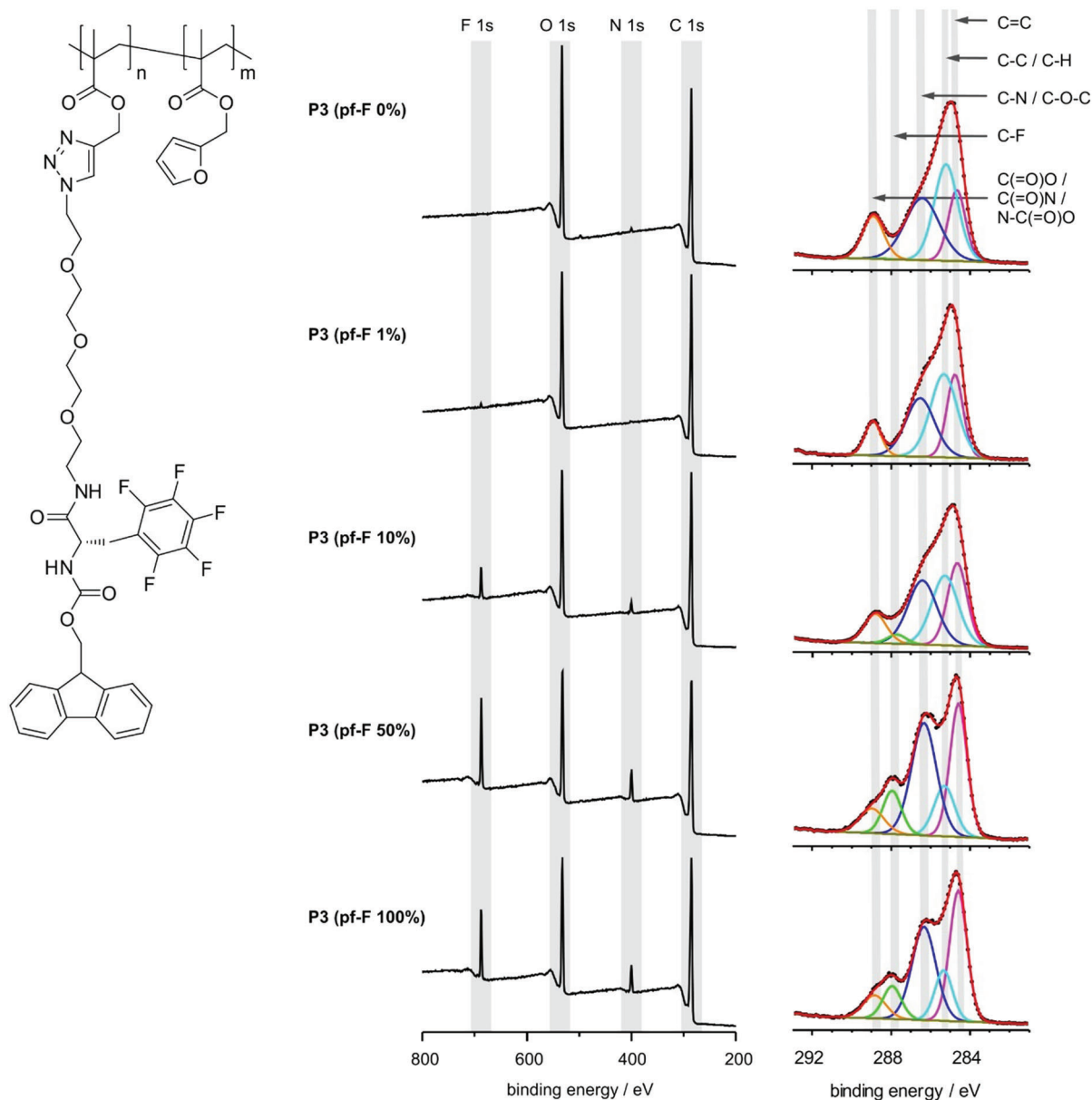


FIGURE 3 Wide scan (middle) and C1s high-resolution (right) XPS spectra of P3 (pf-F) containing varying amounts of pf-F, showing the change in elemental composition and chemical functionalities of the polymer surfaces with changing polymer composition

The percent of pf-F relates to the number of repeat units in the polymer and is therefore not a direct representation of the amount of material (pf-F vs. furan) present in sample. This is of particular importance later on when the mass of the two repeat units (HBP peptide vs. furan) is even larger than for pf-F and furan (Table S5). We therefore converted the theoretical and experimental polymer composition into mass fractions. Details of the mass fraction calculations from XPS data are shown in the supporting information (Section 1.2.3), with the values used shown in Table S6, and results of the calculations are given in Tables S7 and S8. The experimental and theoretical mass fractions are plotted in Figure 4B. A linear correlation ($R^2 > 0.994$) with a statistically relevant (ANOVA, $p < 0.05$) positive association (Pearson's r value > 0.998) between the

experimental and theoretical ratios was observed for all three copolymers from 1%, 10% and 50% pf-F (Table S15). For both ratios, the slope of the linear regression line is close to 1 (0.97 and 0.82 for F/C and N/C, respectively). This suggests that both the polymer composition is likely close to the theoretical composition and that the XPS data are a suitable predictor of the mass fraction of the polymer composition. Moreover, the values for the F/C and N/C data match closely, indicating consistency in the data and that both ratios are representative of the amino acid content, even though the F/C ratio outperforms the N/C ratio slightly in terms of matching the expected and theoretical values.

The data for the homopolymers (0 and 100% pf-F) did not follow that trend. For the P3 (0% pf-F) sample, the deviation could be

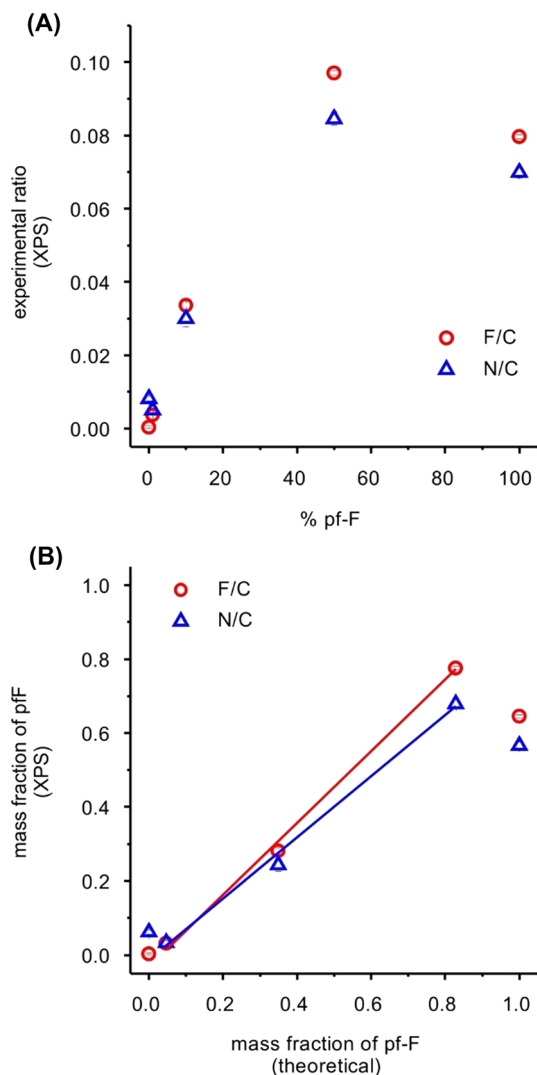


FIGURE 4 Correlation between experimental XPS data and theoretical composition of **P3 (pf-F)** films. (A) F/C and N/C ratios (determined by XPS) as a function of theoretical pf-F content in the polymer films. (B) Mass fraction of pf-F determined from either the F/C or the N/C ratios obtained by XPS and their correlation with the theoretical mass fractions of pf-F. Lines represent linear fits for the data points of the copolymer samples only. Homopolymer samples (0 and 100% pf-F) were excluded from the line fit as they showed behaviour that significantly deviated from that of the copolymers, likely due to the difference in the material synthesis and composition. Errors (included but very small in value) are standard deviations from repeat measurements ($n = 6$). XPS, X-ray photoelectron spectroscopy

explained by the low amount of pf-F present, which may limit the accuracy of the XPS analysis. The significantly lower ratios measured for the **P3 (100% pf-F)** sample suggest that considerably less pf-F was present in the analysed sample volume than expected. The conversion of the alkyne side groups to azides and hence attachment of pf-F was confirmed by ^1H NMR. However, even though the conversion appeared complete by NMR, the sensitivity of this technique is considerably smaller than that of XPS, and XPS is, therefore, more likely to be affected by incomplete functionalisation. This is particularly true

for the homopolymer, as it has been shown before that steric hindrance can prevent full functionalisation of polymer side chains.³⁸

3.2.2 | Linearity and correlation of ToF-SIMS secondary ion intensities with amino acid content

Reliable correlation of ToF-SIMS data with the amount of amino acid or peptide on a surface requires establishment of a predictive relationship between ToF-SIMS secondary ion intensities and the amount of analyte on the surface. Therefore, marker secondary ion intensities from ToF-SIMS for the amino acid and furan components were identified to explore their relationship with the elemental composition derived from XPS data and determine if a linear relationship can be established.

ToF-SIMS spectra for negative and positive polarities of the **P3 (pf-F)** copolymers are shown in Figures S9 and S10 and allowed identification of ions indicative of the pf-F and furan units in the polymers (Table S9). The pf-F unit has characteristic ions for pentafluoro-L-phenylalanine (F^- , C_6F_5^-), Fmoc ($\text{C}_{14}\text{H}_{10}^+$), the short ethylene glycol linker ($\text{C}_2\text{H}_5\text{O}^+$) and the nitrogen-containing functionalities (CN^- , CNO^- and CH_4N^+), whereas the furan ring gives two distinct secondary ions ($\text{C}_4\text{H}_3\text{O}^-$ and $\text{C}_5\text{H}_5\text{O}^+$). The intensity of these ions is shown in more detail in Figures S11 and S12. Images generated from these ions showed uniform chemical distribution (Figures S13 and S14). In this data, it is noticeable that the **P3 (pf-F 0%)** sample contains considerable amounts of sodium, whereas the intensity of the other ions is significantly decreased compared with the copolymer samples. It is possible that this is caused by the difference in the synthetic procedure, as trimethylsilyl deprotection and CuAAC click chemistry were not carried out on this sample.

The normalised intensity of all identified marker ions is plotted against the pf-F content of the sample in Figure S15; a representative selection is shown in Figure 5A. The most robust secondary ion for the monitoring of different pf-F concentration in the polymer films with ToF-SIMS is F^- , as its intensity is relatively strong and increases continuously with pf-F content, and the standard deviations for the data points are small.

Although F^- is a unique marker ion for the model amino acid pf-F, it is not a suitable universal marker ion for peptides. In contrast, nitrogen-containing fragments generated in ToF-SIMS spectra (CN^- , CNO^- and CH_4N^+) are rather generic but can be detected in all peptides. To investigate how suitable these three nitrogen-containing ions are to follow different amounts of peptide on a surface by ToF-SIMS, the F/N ratio (determined by XPS) and the ratio of the F^- ion over each of the three nitrogen-related ions (determined by ToF-SIMS) were plotted against the pf-F content of the samples (Figure S16). These ratios are expected to be independent of the polymer composition, as they only use signals present in pf-F. They can therefore be used as an indicator of how well these nitrogen-containing ions relate to the amount of amino acids/peptides present on the surface. The F/N ratio (XPS) was already

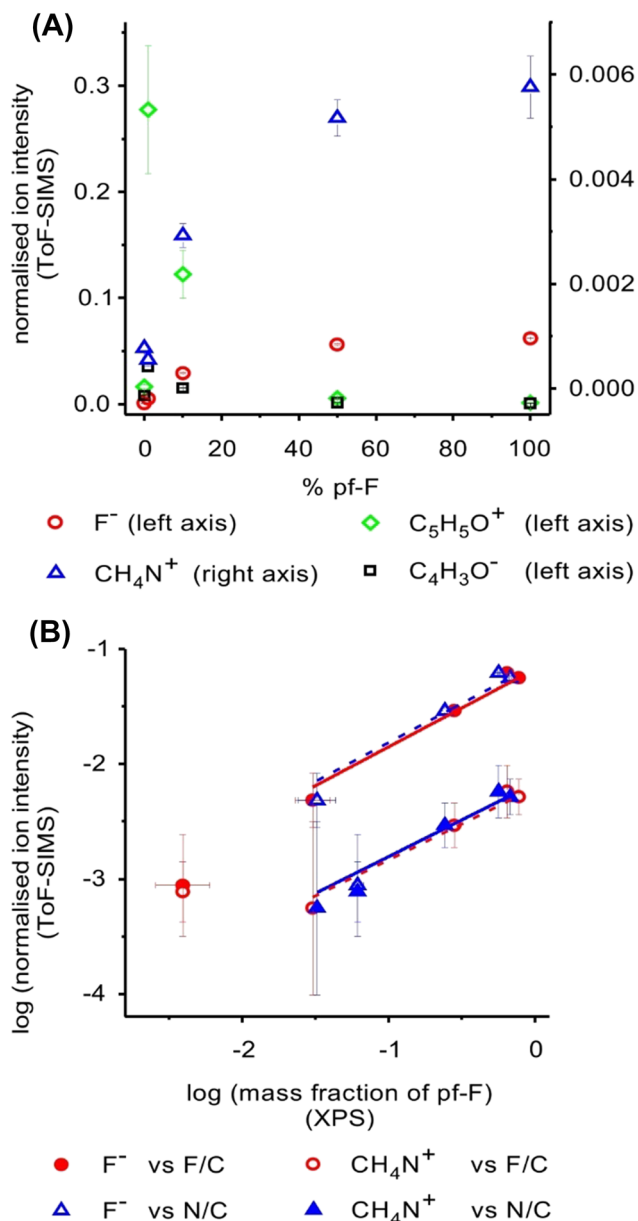


FIGURE 5 Intensities of marker ions for pf-F determined by ToF-SIMS and their relation to the polymer film composition. (A) Normalised (to total ion counts) ion intensities of species associated with pf-F (F^- , CH_4N^+) and furan ($C_4H_3O^-$, $C_5H_5O^+$) for P3 with various pf-F content. (B) Log-log plot of normalised ToF-SIMS ion intensities representative for pf-F (F^- and CH_4N^+) against the mass fraction of pf-F as determined by XPS from either the F/C or the N/C ratio. Lines represent linear fits for the data points of the three copolymer samples only. Errors are standard deviations from repeat measurements (XPS: $n = 6$; ToF-SIMS: $n = 3$). ToF-SIMS, time-of-flight secondary ion mass spectrometry; XPS, X-ray photoelectron spectroscopy

discussed above and shows matching values for polymers with a pf-F content equal or higher than 1% when allowing for the experimental error of the P3 (pf-F 1%) sample (Figure S16A). The F^-/CN^- and F^-/CNO^- ratios increase when the pf-F content increases up to 50%, but then drops for the P3 (pf-F 100%) sample (Figure S16B).

Assuming the F^- ion intensity to be a robust indicator of pf-F content, this indicates that the CN^- and CNO^- ion intensities are either not solely dependent on pf-F concentration or that they display a different matrix effect character compared with the fluoride ion. In contrast, the F^-/CH_4N^+ ion ratio is, within experimental error, constant for all pf-F-containing polymers. CH_4N^+ was therefore selected in addition to F^- for further analysis as a more general marker ion for peptides. As a marker for the furan unit, the $C_4H_3O^-$ ion was chosen over the $C_2H_5O^+$ ion for subsequent data analysis because it displayed less variability (highest standard deviations are 9% and 22% for $C_4H_3O^-$ and $C_2H_5O^+$, respectively).

Normalised secondary ion intensities for pf-F (F^- , CH_4N^+) and furan ($C_4H_3O^-$) associated ions are plotted in Figure 5A. The normalised intensities of F^- (amino acid) increases constantly while that of CH_4N^+ (amino acid) drops from P3 (pf-F 0%) to P3 (pf-F 1%) but then increase continuously with increasing pf-F content. Normalised $C_4H_3O^-$ ion intensities also follow the expected trend of continuous decrease with increasing pf-F content, with the exception of the P3 (pf-F 0%) sample, that has considerably lower $C_4H_3O^-$ ion intensities than the P3 (pf-F 1%) sample.

To relate ToF-SIMS secondary ion intensities with the amount of amino acid on the surface, the ratio of the normalised marker ion intensities was plotted in Figure 5B against the mass fraction of pf-F determined by either using the N/C or the F/C ratio measured by XPS (Section 1.2.3 and Tables S7 and S8). The homopolymer samples display deviating behaviour from the copolymer samples in line with the observations made for the XPS data. Linear regressions for the copolymer datasets were generated both for nonlogarithmic and logarithmic plots; using the coefficient of determination (R^2 value, Table S15), it was found that the F^- and CH_4N^+ ions (amino acid markers) produce the strongest correlation with the experimental mass fraction of pf-F in a log-log plot (Figure 5B) while the $C_4H_3O^-$ and $C_5H_5O^+$ ions (furan markers) produce a better fit to a power law if the normalised secondary ion intensity is plotted on a log scale (Figure S17).

These linear relationships between the logarithm of normalised secondary ion intensities from ToF-SIMS and the logarithm of the mass fraction of pf-F determined from XPS data is strongest for the F^- versus F/C data pair and weakest for the CH_4N^+ versus N/C data pair (Table S15). The stronger association when fluorine-related data (plots involving F^- or F/C values) are used is likely due to the decreased likelihood of contamination or interference from other species with fluorine-related signals. Even though the correlation between nitrogen-based XPS and ToF-SIMS (CH_4N^+ and N/C related) data is statistically slightly weaker than that of fluorine based datasets, the parameters of the regression line, particularly the slope (b), are very similar, suggesting that signals from either fluorine or nitrogen components can be used for the XPS/ToF-SIMS correlation with similar accuracy. Hence, even if the nitrogen related data displays reduced precision, the data in Figure 5 and Table S15 supports its use as a marker for amino acids and peptide surfaces that can be more generically applied than the more specific but artificially introduced fluorine marker.

3.3 | Correlation of HBP content with cell response

The first part of this work provides a platform to establish quantitative SIMS measurements of defined amounts of a model amino acid on polymer films. Applying this technique towards more biologically relevant materials such as peptides allowed us to develop a polymer platform that compares cellular response with quantitative chemical composition, measured before cells are cultured on the surfaces. Our choice to prepare HBP-polymer films was due to the participation of this class of peptides in cell-cell adhesion and cell-matrix interactions.¹³ We hypothesised that polymer films with varying HBP content would result in differences in the adhesion of hESCs that can be quantitatively described by correlation of XPS and ToF-SIMS data of the surface acquired before cell culture to explore the ability to use ToF-SIMS data for quantitative correlation in biology.

3.3.1 | Preparation of HBP-containing polymers

To prepare HBP-containing polymers, the same alkyne and furan containing copolymers designed for the previous pf-F study (P2) were used and functionalised with an azide containing HBP (Figure S1).

As the response of hESCs has previously been shown to be enhanced by small quantities of surface bound peptides,¹³ polymers in which HBP makes up 1%, 5% or 10% of the side chains were prepared. Homopolymers were not included in this study as the pf-F study showed that the homopolymers deviate significantly from the linear correlations observed for the copolymers.

The HBP-containing copolymers were analysed by NMR (Figure S18). The ¹H NMR showed an increase of peptide-binding domain signals from 1% to 10% HBP and a decrease of the furan associated peak. Due to the complexity of the HBP spectrum and the overlay of HBP signals with most of the copolymer signals, no further analysis of the NMR data was undertaken.

3.3.2 | XPS analysis of HBP-containing polymer films

XPS spectra of the P3 (HBP) samples showed the presence of carbon, oxygen and nitrogen, but also strong signals for fluorine (Figure S19 and Table S10). As neither the HBP peptide nor the polymer contains fluorine, the most likely reason for the presence of fluorine is residual trifluoroacetic acid, which was used in the synthesis of HBP to remove the side chain protection groups and subsequently be present as the counter anion to the basic amino acid residues in HBP.

Following the increase in the number of nitrogen present with increasing amount of HBP in the polymer, the relative amount of nitrogen measured by XPS increased from P3 (HBP 1%) to P3 (HBP 10%) (Table S10). This indicates that the HBP modification was successful and that the samples indeed display increasing amounts of HBP.

The theoretical and experimental N/C ratio was computed (Table S11) and plotted against each other in Figure S20. The experimental values show very high correlation (Pearson's r value = 0.999) with high statistical significance (ANOVA, p value = 0.009) (Table S15); however, compared with the correlation obtained from the P3 (pf-F) samples (Figure S8), the slope of the correlation for the P3 (HBP) samples is considerably smaller further away from unity. This could mean that for the P3 (HBP) samples, the experimental N/C ratio underestimates the amount of peptide present. Alternatively, it is possible that functionalisation of the polymer via the CuAAC reaction was not quantitative. Incomplete conversion would be difficult to detect due to the small amount of alkyne present in the polymer, making it challenging to quantitatively measure conversion via NMR. The larger size of HBP compared with pf-F may further contribute to a reduced conversion for HBP. Given the very good correlation found between theoretical and experimental N/C values, incomplete conversion is the more likely factor responsible for the deviation between the values. This, in turn, makes it imperative to undertake further correlations related to HBP content using experimental values rather than theoretical ones.

3.3.3 | ToF-SIMS analysis of HBP containing polymer films

ToF-SIMS analysis of the three HBP-containing copolymers focused on the two marker ions identified from the P3 (pf-F) analysis: CH_4N^+ for the amino acids and $\text{C}_5\text{H}_5\text{O}^+$ for furan. The ToF-SIMS spectra are shown in Figure S21, showing the presence of both CH_4N^+ and $\text{C}_5\text{H}_5\text{O}^+$ ions. These ions are uniformly distributed across the surface (Figure S22A) except for $\text{C}_5\text{H}_5\text{O}^+$ on P3 HBP 10% that showed micro-scale structuring. Areas of low intensity in these images correspond to areas of high intensity of Na^+ and K^+ (Figure S23), indicating that salt formation, possibly originating from salts introduced through the higher HBP peptide content, is a likely cause for these structures. The CH_4N^+ ion increases with increasing HBP content but the $\text{C}_5\text{H}_5\text{O}^+$ ion does not show a trend that follows the HBP content (Figures S22B and S24).

Following the identification of the logarithm of the mass fraction and secondary ion intensities as suitable means to explore linear correlations between ToF-SIMS and XPS data in the previous section, log-log plots of the normalised CH_4N^+ and $\text{C}_5\text{H}_5\text{O}^+$ ion intensities and the mass fraction of HBP determined using the N/C ratio were generated. The calculations are detailed in Section 2.2.4 in the supporting information, the data used are provided in Table S12, results of the calculations are given in Table S13 and the final plot is shown in Figure S25. Although a linear trendline with acceptable fit ($R^2 > 0.85$) and high correlation (Pearson's r value > 0.96) can be placed through the data, the correlation is not statistically significant (ANOVA, $p > 0.1$) (Table S15). A likely reason for this is the higher variability of the nitrogen related datasets (N/C ratio and CH_4N^+). Particularly, the N/C ratio and the associated mass fraction for P3 (HBP) samples display larger errors and variability. In contrast, the ToF-SIMS

secondary ion data show considerably smaller errors, suggesting that ToF-SIMS data could be more suitable for quantitative analysis in this particular case.

3.3.4 | hESC culture on HBP containing polymer surface

hESCs were cultured on the P3 (HBP) samples to investigate the response of these cells to different amounts of HBP on the surface, using Matrigel as a reference sample. Matrigel is widely used as a cell support. It contains laminin, entactin and other structural proteins that provide cell support through a variety of adhesive peptide sequences; however, the heterogeneous nature of the material makes it challenging to isolate the effect of any particular component and can lead to batch-to-batch variability and variable cell response. The P3 (HBP) polymer system used here is therefore not only interesting as a model system for surface analysis but also provides a means to study the role of a single peptide sequence on cell response.

hESCs were cultured on the samples and cell counts were performed after 24 and 72 h (Figure 6 and Table S14). Cell numbers were statistically different between all samples at both timepoints, except for the P3 (HBP 1%) and P3 (HBP 5%) samples, for which the difference was not statistically significant.

The hESCs densely populate the Matrigel surface as well as the P3 (HBP 5%) and P3 (HBP 10%) samples (Figure 6A). On the P3 (HBP

1%) sample, coverage after 24 h is not complete. At 24 h, the P3 (HBP 1%) sample is also the sample with lowest cell count. The number of cells increases with increasing HBP content in the copolymer at 24 h but does not show a directional trend with HBP content after 72 h of culture. This may be due to a higher importance of the presence of cell adhesion domains at early timepoints when cells need to establish adhesions with the substrate.

Cells expand and become confluent after 24 h of culture on Matrigel, indicating that the material provides a good support for attachment and development of hESCs. In the 1% HBP cells attach, however, growth appears to be localised. This suggests that there is a heterogeneous distribution of HBP; however, ToF-SIMS images of this ratio in Figure S22 indicate a uniform coverage markers attributed to peptide (CH_3N_2^+ , $\text{C}_5\text{H}_{10}\text{N}^+$, CN^- and CNO^-). The 5% and 10% HBP ratios hESCs attach and expand reached confluency after 24 h of culture. This suggests that the amount of peptide on the surface is sufficient to facilitate adhesion. Average cell count after 24 h shows a reduced cell number when compared with Matrigel. However, after 72 h of culture, comparable cell numbers are observed for 1% and 10% HBP. Following 72 h of culture on 10% HBP-coated substrates, NANOG, SOX2 and OCT4 staining for pluripotency and self-renewal marker expression indicated that increased cell numbers between 24 and 72 h was due to expansion and not differentiation. Staining of hESCs for pluripotent marker expression after 72 h (Figure S26) shows that hESCs maintain pluripotency, supporting the assumption that the observed increase in cell count from 24 to 72 h is due to cell expansion rather than cell differentiation.

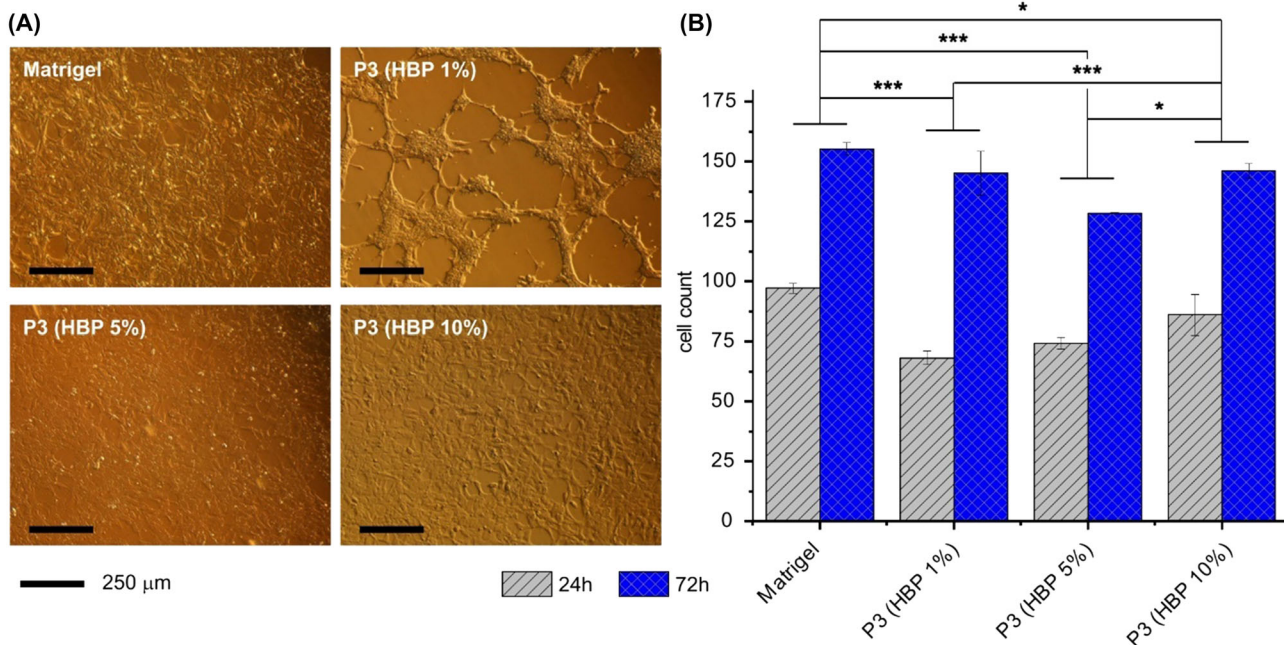


FIGURE 6 Cellular response to substrate chemistries. (A) Representative photomicrographs illustrate differing levels of human embryonic stem cell (hESC) attachment to substrates after 24 h. Scale bar = 250 μm. (B) Higher hESC number was seen on furan polymers when coated with heparin-binding peptide after 24 h of attachment and 72 h of culture. Errors are standard deviations from repeat measurements ($n = 3$). HBP, heparin-binding peptide

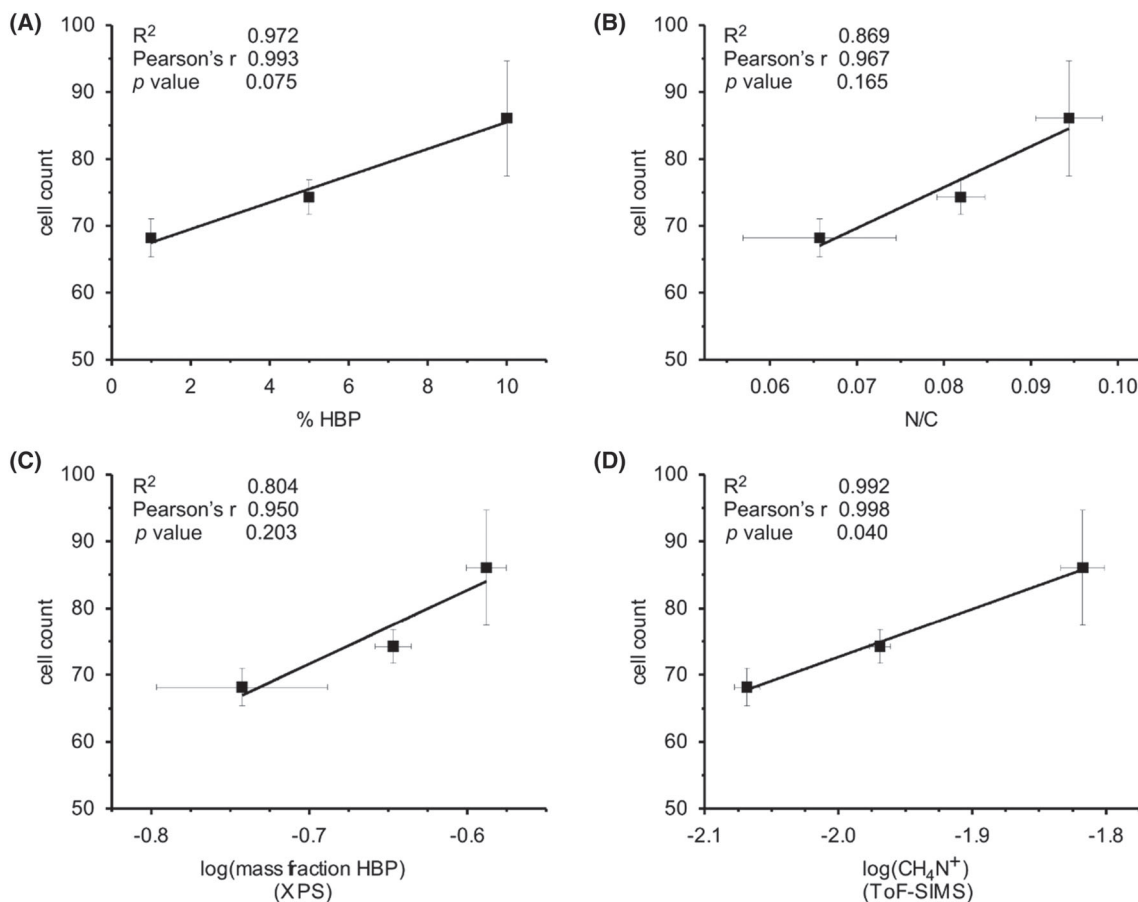


FIGURE 7 Comparison of the degree of association of the cell count after 24 h with (A) %HBP, (B) N/C ratio determined by XPS, (C) logarithm of the mass fraction HBP derived from the N/C ratio and (D) the logarithm of the normalised CH₄N⁺ ion intensity obtained from ToF-SIMS. Linear regressions were generated for each dataset and the coefficient of correlation (r^2 , goodness of fit), Pearson's r value (strength and direction of association) and the statistical significance (p value, ANOVA) are reported. Errors are standard deviations from repeat measurements (XPS: $n \geq 4$; ToF-SIMS: $n = 3$; cell count: $n = 3$). HBP, heparin-binding peptide; ToF-SIMS, time-of-flight secondary ion mass spectrometry; XPS, X-ray photoelectron spectroscopy

3.3.5 | Correlation between cell count and ToF-SIMS data

The cell data suggest that the P3 (HBP) samples are able to induce differential cell response (cell count) at early timepoints (24 h of culture). Therefore, the surface analysis data were correlated with the 24-h cell data to determine the suitability of XPS- and ToF-SIMS-derived data to establish correlations between cell response.

The theoretical polymer composition (%HBP) experimental XPS data (N/C ratio and the log [mass fraction]) and experimental ToF-SIMS data (logarithm of the normalised CH₄N⁺ ion intensity) were plotted against the cell count at 24 h (Figure 7). Both XPS related plots did not yield a statistically significant correlation (ANOVA, $p > 0.1$; Table S15), likely due to the large error associated with this XPS dataset. The %HBP and log (CH₄N⁺) datasets both yield high associations (Pearson's r value = 0.993 and 0.998, respectively) and high correlation to a linear trendline ($R^2 = 0.972$ and 0.992, respectively). Although these associations are significant for both datasets, the log (CH₄N⁺) data display a considerably higher statistical

significance (ANOVA, $p = 0.040$) than the %HBP dataset (ANOVA, $p = 0.075$). It can therefore be concluded that not only can ToF-SIMS secondary ion data be used quantitatively to establish correlations with cell data but it may also be able to do so with higher precision than XPS if only generic signals are available for compound identification.

4 | CONCLUSIONS

This work presents the establishment of a material design approach based on controlled RAFT polymerisation and subsequent CuAAC reaction that enables excellent control over the amount of amino acid incorporated into a polymer and presented onto a surface. Although the system works well for a single amino acid, longer peptide sequences likely suffer from reduced conversion.

Use of a fluorine containing model amino acid and comparison with the fluorine-related signals of the label demonstrated that nitrogen-based signals from XPS (N/C ratio) and ToF-SIMS (CH₄N⁺)

provide comparable and quantifiable ways to parametrise the amino acid and peptide content on the surface of the polymer films. Correlations between XPS and ToF-SIMS datasets were found to be most significant when plotting the logarithm of the secondary ion intensity against the mass fraction of the amino acid, derived from conversion of the N/C or F/C values obtained by XPS. This demonstrates that ToF-SIMS secondary ion intensities have the potential to be used for quantitative parametrisation of amino acid or peptide content on surfaces after minimal processing, making it accessible for routine analysis by non-specialists.

When investigating linearity and association between surface analytical data, the homopolymer samples consistently displayed deviations from linearity compared with the copolymer samples. It must therefore be concluded that although homopolymers may still be suitable reference materials for biological experiments, when aiming to establish systematically varying trends of physicochemical properties, the polymer system we designed only operates well if used as a copolymer. This finding could be of relevance to other polymer systems, and we advise that care should be taken when combining homopolymer and copolymer surface analysis data for the investigation of systematic trends.

Our copolymer system provided a suitable platform to study the influence of varying amounts of HBP on the maintenance of self-renewal capability of hESCs. hESCs maintained their self-renewal capability on the HBP-containing copolymers over 72 h of culture. In addition, cell adhesion increased with increasing HBP content in the copolymer, which was shown to correlate to the logarithm of the normalised CH_4N^+ ion intensity measured by ToF-SIMS with high statistical significance. The system developed here may provide opportunities towards a scalable platform for the expansion of hESCs to improve hESC availability for subsequent biomedical applications.

ACKNOWLEDGEMENTS

This work is submitted to this issue in memory of Martin Seah to mark the support he offered to surface analysis in The School of Pharmacy and more widely The University of Nottingham. Martin encouraged links between NPL and Nottingham, writing a letter supporting the bid by Martyn Davies for the first SIMS instrument in the School of Pharmacy in the early 1990s. He understood the importance of surface analysis research in the pharmaceutical and biomedical sector and attended our conferences encouraging NPL staff to collaborate, with Ian Gilmore becoming a visiting professor in the School of Pharmacy. This link has engendered incredibly productive metrological, pharmaceutical and biomaterials research collaborations, between the organisations most recently resulting in the 3D OrbISIMS (Passarelli Nature Methods 2017). This paper is a good example of the combination of Nottingham and NPL interests, which are one of Martin's legacies.

This work was supported by EURAMET through an EMRP Researcher Grant (Grant HLT04-REG4) and the Chemical and Biological Programme of the National Measurement System. The EMRP is jointly funded by the EMRP participating countries within EURAMET

and the European Union. M.L. was supported by the Leverhulme Trust (Grant RPG-2016-199), and M.T. and A.C. were supported by the EPSRC CTD in Regenerative Medicine (Grant EP/F/500491/1). We are grateful to Caterina Minelli for useful comments on the manuscript.

CONFLICT OF INTEREST

The authors declare that there are no conflicts of interest.

AUTHOR CONTRIBUTIONS

Conceptualisation and project administration were done by M.Z., M.A. and A.S., and the methodology was designed by F.S. and M.Z. The investigation was carried out by F.S., M.T., J.M., J.S., S.J.S., and R.S.; S.G., R.S., S.J.S., and A.S. provided resources; and formal analysis was conducted by M.Z., F.S., M.T., J.M., A.C., J.S., M.L., and S.J.S. M.Z., F.S., M.T., S.J.S., J.S. and J.M. were responsible for data curation, and M.Z., F.S. and M.T. undertook data validation. The work was supervised by M.Z., S.S., M.A., A.S., C.D. and W.C. The data were visualised by M.Z., F.S., M.T., J.M., M.L. and A.C. M.Z., M.T. and F.S. wrote the original draft, and all authors contributed to review and editing of the manuscript. M.Z., D.S., M.A. and A.S. were involved in funding acquisition.

ORCID

Weng C. Chan  <https://orcid.org/0000-0002-0488-825X>

Alexander G. Shard  <https://orcid.org/0000-0002-8931-5740>

Morgan R. Alexander  <https://orcid.org/0000-0001-5182-493X>

Mischa Zelzer  <https://orcid.org/0000-0002-6086-2206>

REFERENCES

- Leipzig ND, Shoichet MS. The effect of substrate stiffness on adult neural stem cell behavior. *Biomaterials*. 2009;30(36):6867-6878.
- Discher DE, Janmey P, Wang Y-I. Tissue cells feel and respond to the stiffness of their substrate. *Science*. 2005;310(5751):1139-1143.
- Trappmann B, Gautrot JE, Connelly JT, et al. Extracellular-matrix tethering regulates stem-cell fate. *Nat Mater*. 2012;11(7):642-649.
- Benoit DSW, Schwartz MP, Durney AR, Anseth KS. Small functional groups for controlled differentiation of hydrogel-encapsulated human mesenchymal stem cells. *Nat Mater*. 2008;7(10):816-823.
- Tsou Y-H, Khoneisser J, Huang P-C, Xu X. Hydrogel as a bioactive material to regulate stem cell fate. *Bioact Mater*. 2016;1(1):39-55.
- Yang C, Tibbitt MW, Basta L, Anseth KS. Mechanical memory and dosing influence stem cell fate. *Nat Mater*. 2014;13(6):645-652.
- Yang X, Al Hegy A, Gauthier ER, Gray-Munro J. Influence of mixed organosilane coatings with variable RGD surface densities on the adhesion and proliferation of human osteosarcoma Saos-2 cells to magnesium alloy AZ31. *Bioactive Materials*. 2017;2(1):35-43.
- Adamus A, Komasa J, Kadłubowski S, et al. Thermoresponsive poly[tri(ethylene glycol) monoethyl ether methacrylate]-peptide surfaces obtained by radiation grafting-synthesis and characterisation. *Colloids Surf B Biointerfaces*. 2016;145:185-193.
- Clauder F, Möller S, Köhling S, et al. Peptide-mediated surface coatings for the release of wound-healing cytokines. *J Tissue Eng Regen Med*. 2020;14(12):1738-1748.
- Santiago LY, Nowak RW, Peter Rubin J, Marra KG. Peptide-surface modification of poly (caprolactone) with laminin-derived sequences for adipose-derived stem cell applications. *Biomaterials*. 2006;27(15):2962-2969.

11. Melkoumian Z, Weber JL, Weber DM, et al. Synthetic peptide-acrylate surfaces for long-term self-renewal and cardiomyocyte differentiation of human embryonic stem cells. *Nat Biotechnol.* 2010;28(6):606-610.
12. Ishihara J, Ishihara A, Fukunaga K, et al. Laminin heparin-binding peptides bind to several growth factors and enhance diabetic wound healing. *Nat Commun.* 2018;9(1):2163.
13. Klim JR, Li L, Wrighton PJ, Piekarczyk MS, Kiessling LL. A defined glycosaminoglycan-binding substratum for human pluripotent stem cells. *Nat Methods.* 2010;7(12):989-994.
14. Wang Q, Jakubowski JA, Sweedler JV, Bohn PW. Quantitative submonolayer spatial mapping of Arg-Gly-Asp-containing peptide organomeraptan gradients on gold with matrix-assisted laser desorption/ionization mass spectrometry. *Anal Chem.* 2004;76(1):1-8.
15. Zelzer M, Majani R, Bradley JW, Rose FRAJ, Davies MC, Alexander MR. Investigation of cell-surface interactions using chemical gradients formed from plasma polymers. *Biomaterials.* 2008;29(2):172-184.
16. Stevens JS, de Luca AC, Downes S, Terenghi G, Schroeder SLM. Immobilisation of cell-binding peptides on poly- ϵ -caprolactone (PCL) films: a comparative XPS study of two chemical surface functionalisation methods. *Surf Interface Anal.* 2014;46(10-11):673-678.
17. Apte JS, Collier G, Latour RA, Gamble LJ, Castner DG. XPS and ToF-SIMS investigation of α -helical and β -strand peptide adsorption onto SAMs. *Langmuir.* 2010;26(5):3423-3432.
18. Chittur KK. FTIR/ATR for protein adsorption to biomaterial surfaces. *Biomaterials.* 1998;19(4):357-369.
19. Sahoo JK, Sirimuthu NMS, Canning A, Zelzer M, Graham D, Ulijn RV. Analysis of enzyme-responsive peptide surfaces by Raman spectroscopy. *Chem Commun.* 2016;52(25):4698-4701.
20. Shard AG. Detection limits in XPS for more than 6000 binary systems using Al and Mg K α X-rays. *Surf Interface Anal.* 2014;46(3):175-185.
21. Stevens JS, de Luca AC, Pelendritis M, Terenghi G, Downes S, Schroeder SLM. Quantitative analysis of complex amino acids and RGD peptides by X-ray photoelectron spectroscopy (XPS). *Surf Interface Anal.* 2013;45(8):1238-1246.
22. Laromaine A, Koh L, Murugesan M, Ulijn RV, Stevens MM. Protease-triggered dispersion of nanoparticle assemblies. *J Am Chem Soc.* 2007;129(14):4156-4157.
23. Zelzer M, Scurr DJ, Alexander MR, Ulijn RV. Development and validation of a fluorescence method to follow the build-up of short peptide sequences on solid 2D surfaces. *ACS Appl Mater Interfaces.* 2012;4(1):53-58.
24. Lopez LC, Gristina R, Ceccone G, Rossi F, Favia P, d'Agostino R. Immobilization of RGD peptides on stable plasma-deposited acrylic acid coatings for biomedical devices. *Surf Coat Technol.* 2005;200(1):1000-1004.
25. Zelzer M, McNamara LE, Scurr DJ, Alexander MR, Dalby MJ, Ulijn RV. Phosphatase responsive peptide surfaces. *J Mater Chem.* 2012;22(24):12229-12237.
26. Kotowska AM, Trindade GF, Mendes PM, et al. Protein identification by 3D OrbiSIMS to facilitate in situ imaging and depth profiling. *Nat Commun.* 2020;11(1):5832.
27. Aoyagi S, Fujiwara Y, Takano A, et al. Evaluation of time-of-flight secondary ion mass spectrometry spectra of peptides by random forest with amino acid labels: results from a versailles project on advanced materials and standards interlaboratory study. *Anal Chem.* 2021;93(9):4191-4197.
28. Awaja F. Multivariate calibration of ToF-SIMS and XPS data from plasma-treated polypropylene thin films. *Plasma Processes Polym.* 2014;11(8):745-754.
29. Shard AG, Spencer SJ, Smith SA, Havelund R, Gilmore IS. The matrix effect in organic secondary ion mass spectrometry. *Int J Mass Spectrom.* 2015;377:599-609.
30. Ray S, Steven RT, Green FM, et al. Neutralized chimeric avidin binding at a reference biosensor surface. *Langmuir.* 2015;31(6):1921-1930.
31. Pei Y, Cant DJH, Havelund R, et al. Argon cluster sputtering reveals internal chemical distribution in submicron polymeric particles. *J Phys Chem C.* 2020;124(43):23752-23763.
32. Briggs D, Brewis DM, Dahm RH, Fletcher IW. Analysis of the surface chemistry of oxidized polyethylene: comparison of XPS and ToF-SIMS. *Surf Interface Anal.* 2003;35(2):156-167.
33. Beer MV, Hahn K, Diederichs S, et al. Quantifying ligand-cell interactions and determination of the surface concentrations of ligands on hydrogel films: the measurement challenge. *Biointerphases.* 2015;10(2):021007.
34. Semsarilar M, Ladmiraal V, Perrier S. Highly branched and hyperbranched glycopolymers via reversible addition-fragmentation chain transfer polymerization and click chemistry. *Macromolecules.* 2010;43(3):1438-1443.
35. Seah MP. A system for the intensity calibration of electron spectrometers. *J Electron Spectrosc Relat Phenomena.* 1995;71(3):191-204.
36. Wagner MS, Castner DG. Characterization of adsorbed protein films by time-of-flight secondary ion mass spectrometry with principal component analysis. *Langmuir.* 2001;17(15):4649-4660.
37. Cowie JM, Arrighi V (Eds). *Polymers: Chemistry and Physics of Modern Materials.* 3rd ed. CRC Press; 2008.
38. Akhtar Hussain Malik SH, Chowdhury SR, Iyer PK. Conjugated polymers for disease diagnosis and theranostics medicine. In: Liu BL, ed. *Conjugated Polymers for Biological and Biomedical Applications.* Wiley; 2018:321-358.

SUPPORTING INFORMATION

Additional supporting information may be found in the online version of the article at the publisher's website.

How to cite this article: Taylor M, Simoes F, Smith J, et al. Quantifiable correlation of ToF-SIMS and XPS data from polymer surfaces with controlled amino acid and peptide content. *Surf Interface Anal.* 2022;1-16. doi:10.1002/sia.7052